Off-line Scan Path Planning for Robotic NDT

M. Morozov, S. G. Pierce, Ch. N. MacLeod, C. Mineo and R. Summan
Department of Electronic and Electrical Engineering, University of Strathclyde
Technology & Innovation Centre, 99 George Street, Glasgow, G1 1RD, UK
+44 (0)141 444 7406
Maxim.Morozov@strath.ac.uk

Abstract

This work presents computer-aided scan path generation for robotic non-destructive testing of complex shaped test-pieces. Off-line programmed scan path was used to robotically inspect an aluminium fixed leading edge skin panel of an aircraft wing by means of swept frequency eddy currents method. Eddy currents probe was deployed by means of a six-axis robotic arm KUKA KR5 arc. Reverse engineering of the test-piece was carried out to reconstruct CAD model of its surface. Positioning accuracy of the performed continuous scan was measured with a laser tracker in accordance with ISO 9283:1998 and is reported in the paper. The positional uncertainty of the NDT scan calculated as the standard deviation of the measured path coordinates from the command path coordinates does not exceed 0.5 mm which is rather moderate taking in account uncertainties associated with the off-line robot programming.

Keywords. Eddy Current NDT, robotics, off-line path planning, path accuracy, reverse engineering.

1. Introduction

Compared to manual Non-Destructive Testing (NDT) for inspection of engineering components, automated robotic deployment of the same NDT techniques offers an increase in accuracy, precision and speed of inspection while reducing production time and associated labour costs. Traditionally, the robot scan path is either taught or programmed manually. Automation of NDT scan path generation, as presented in this

paper, offers further significant time reduction, and an increase in the flexibility of inspection planning compared to manual robot teaching and programming, and this is the main contribution of this work. Moreover, such a solution helps to maintain a controlled probe orientation with respect to the scanned surface, dramatically reducing lift-off noise. Automation of NDT of engineering components and structures represents one of the strategic objectives of many industries. The principal users of NDT are the automotive, aerospace, petrochemical and power generation industries. Inspection of numerous components (for instance, in automotive manufacturing) or extended structures (for instance, aircraft skin) is laborious and time consuming. Some NDT techniques, such as visual inspection, eddy currents testing (ECT) and ultrasonic testing (UT) can be readily automated and there has recently been a growing interest in the development of robotic systems for NDT.

A number of previous researchers have explored robotic NDT delivery using both mobile and fixed robotic platforms, and considerable expertise has already been demonstrated by partners in the UK Research Centre for Non-Destructive Evaluation (RCNDE) [1] – particularly in the aerospace sector. A combination of mobile robotics with a seven axis arm for ultrasonic and eddy current inspection has been explored at London South Bank University [2]. Partnership between QinetiQ & Sonatest drove the development of the Boeing Mobile Automated Scanner (MAUS) and TRECSCAN [3], to produce a transient eddy-current scanner with scan speeds of around 9 m^2 per hour (with 1 mm resolution). A more recent development of this technology with Diagnostic Sonar has concentrated on high speed ultrasonic array imaging using a relatively low cost ultrasonic array driver platform developed in conjunction with National Instruments (FlawInspecta) [4]. A further development to this collaboration was the NSpect Robotic Non-Destructive Inspection cell developed by Genesis Systems [5, 6]. Incorporating ANDSCAN and FlawInspecta technology, the NSpect system employs a KUKA 6DOF robot arm to perform “part to process”, or “process to part” ultrasonic inspection using either an immersion tank scan, or a recirculating water couplant. The IntACom project has produced a prototype robotic NDT system capable of inspecting complex geometry composite components with great time savings by means of two 6-axis robotic arms carrying Phased Array Ultrasonic Testing (PAUT) probes [7].

Outwith RCNDE work has included a six Degrees of Freedom (DOF) robotic arm (Mitsubishi MELFA RV-1A), used for robotic scanning of various test pieces by means of eddy current (EC) technique [8, 9]. A seven-axis robotic arm transportable by climbing and walking robots (CLAWAR) was developed to deploy NDT probes to perform inspection of very large and critical infrastructure located in hazardous environments [10]. The EloScan system using a six DOF heavy-duty industrial robot KUKA KR 15/2 has been designed for the eddy-current inspection of rotationally symmetrical components of aircraft engines [11]. Due to its universal design the system is claimed to be able to scan complex geometries that require precise probe guidance and a high repeating accuracy. The "ROBOSKOP" VT-3000 is intended for testing of a wide range of parts and provides quick probes changeover for various techniques and adaptation to different forms and dimension types of testing objects. The Tecnatom SIROCO-RABIT control system for industrial robots allows simultaneous and coordinated control of two robots for ultrasonic inspection in transmission and pulse-echo mode. The Sysaxe NDT developed a robotized cell based on 6 axis industrial robots to perform UT or EC NDT inspections with contour following features. The Sysaxe NDT cells are offered in single (one robot) or Dual (twin synchronized robots) architecture. Multi-axis robots using multiple end effector tools and phased array ultrasound technology have been developed by General Electric for robotic inspection of fibre reinforced composites [12, 13].

Traditionally, the robot scan path is either taught or programmed manually. Automation of NDT scan path generation, as presented in this paper, offers further significant time reduction, and increase in flexibility of inspection planning compared to manual robot teaching and programming. Moreover, such a solution helps to maintain a controlled probe orientation with respect to the scanned surface, and thus dramatically reducing lift-off noise. Scan path planning can be performed either using general purpose CAM software or proprietary tools developed for particular NDT application [14]. Offline robot programming offers the robot programmer a number of key benefits, most notably a reduction in the time it takes to design and program an automated robotic system thus reducing production downtimes [15, 16]. However, significant errors can occur in an

off-line generated toolpath due to deviations of individual robot characteristics (machining tolerances in the robot linkages, compliance and elasticity in the robot arm, encoder resolution, and the lack of repeatability during calibration) from the general kinematic model [17].

A significant problem in the field of production line automation is the design of flexible and autonomous robotic systems able to manipulate complex objects. Most current systems depend on complete knowledge of both the shape and position of the parts. When CAD data for the part are not available, there is a need for efficient and accurate reverse engineering. An additional problem arises in the fact that real parts often deviate from their respective CAD models. This, combined with intrinsic errors of off-line robot programming explicated above, creates strong necessity for adaptive control of scan path with metrology feedback.

Our study aims to explore the capability for fully automated NDT scan-path generation using an approach implemented through Mastercam & Robotmaster software. This paper will be of interest to specialists in the field of NDT automation.

2. Computer-Aided Scan Path Planning

2.1 Reverse Engineering

When a CAD model of a test-piece is not available, a coordinate measuring machine (CMM), such as FaroArm, equipped with a Laser Line Probe (LLP) or a contact probe, can be used to reconstruct its surface by means of metrology software (e.g. Verisurf). In this study we use fixed leading edge skin panel of an aircraft wing made from AL-2014A-T4 as an example of a complex geometry test-piece, shown in Figure 1. The sample featured numerous fastener hole with and without inserted rivets. A dense point cloud was acquired using LLP. The point cloud was filtered to produce homogeneous spacing of 1mm between neighbouring points. Then, a mesh was generated and smoothed. The part surface was reconstructed using vertical spline slicing approach. Each spline had 50 points. The accuracy map of the reverse engineered CAD model of

the leading edge skin panel with respect to the acquired point cloud is illustrated in Figure 2. The standard deviation of the reconstructed surface from the pointcloud acquired using FaroArm with LLP is circa 100 μm.

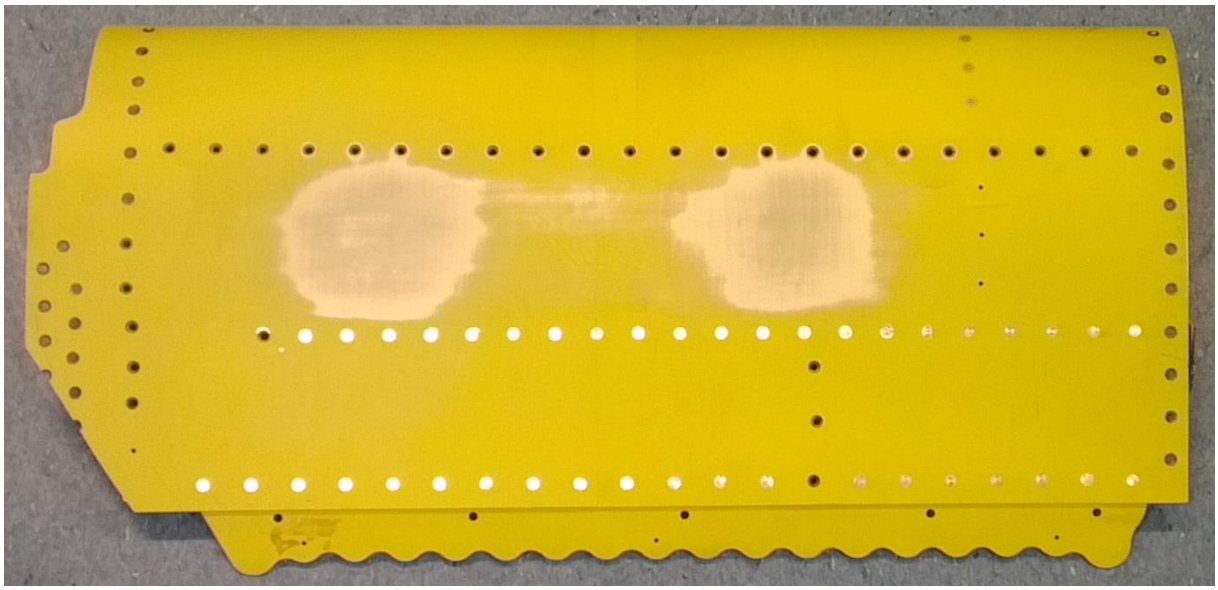

Figure 1. Riveted fixed leading edge skin panel made from AL-2014A-T4

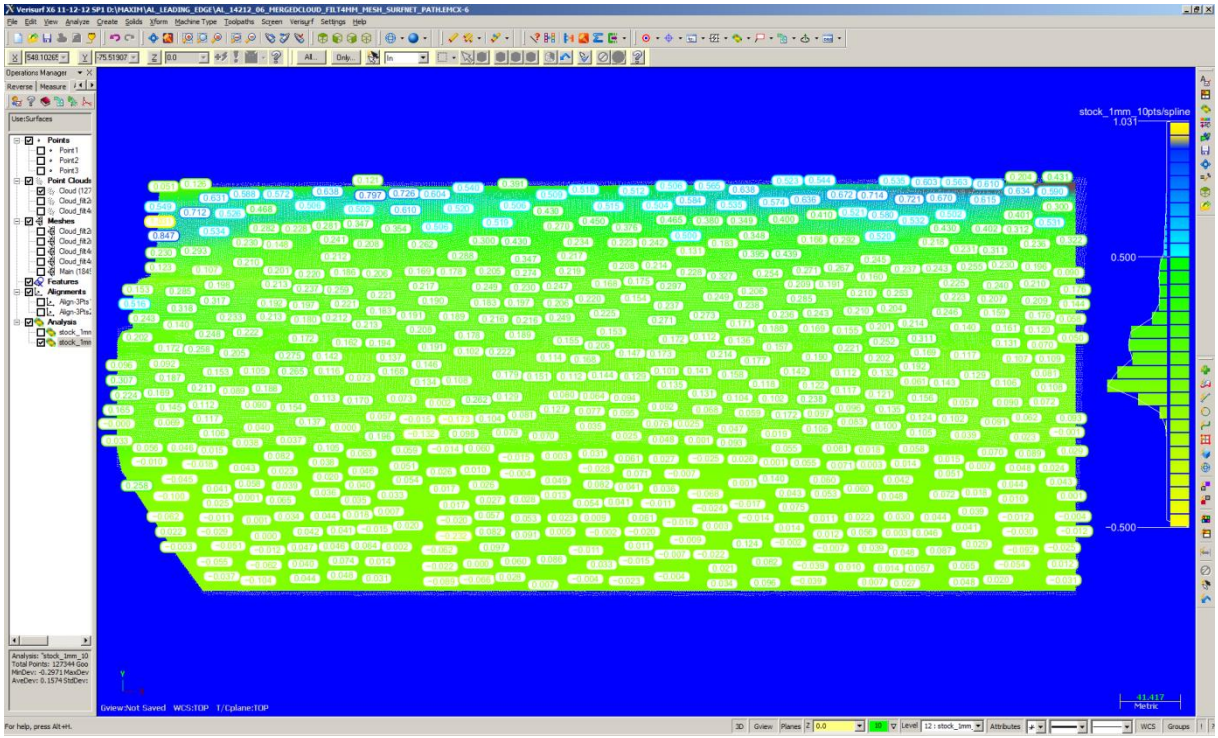

Figure 2. Accuracy map of the reverse engineered leading edge skin

2.2 Computer-Aided Scanpath Generation by means of Commercial Software

A scan path for the reverse engineered edge skin panel was generated in MasterCAM X6 software, which offers fine controls, flexibility and compatibility with standard machining operations. The scan path had a topology of meander. The principal direction of scan was X, with distance between scan passes being 2 mm which was a compromise between spatial resolution and the total time of scan. The scan resolution along scan lines was approximately 2 mm.

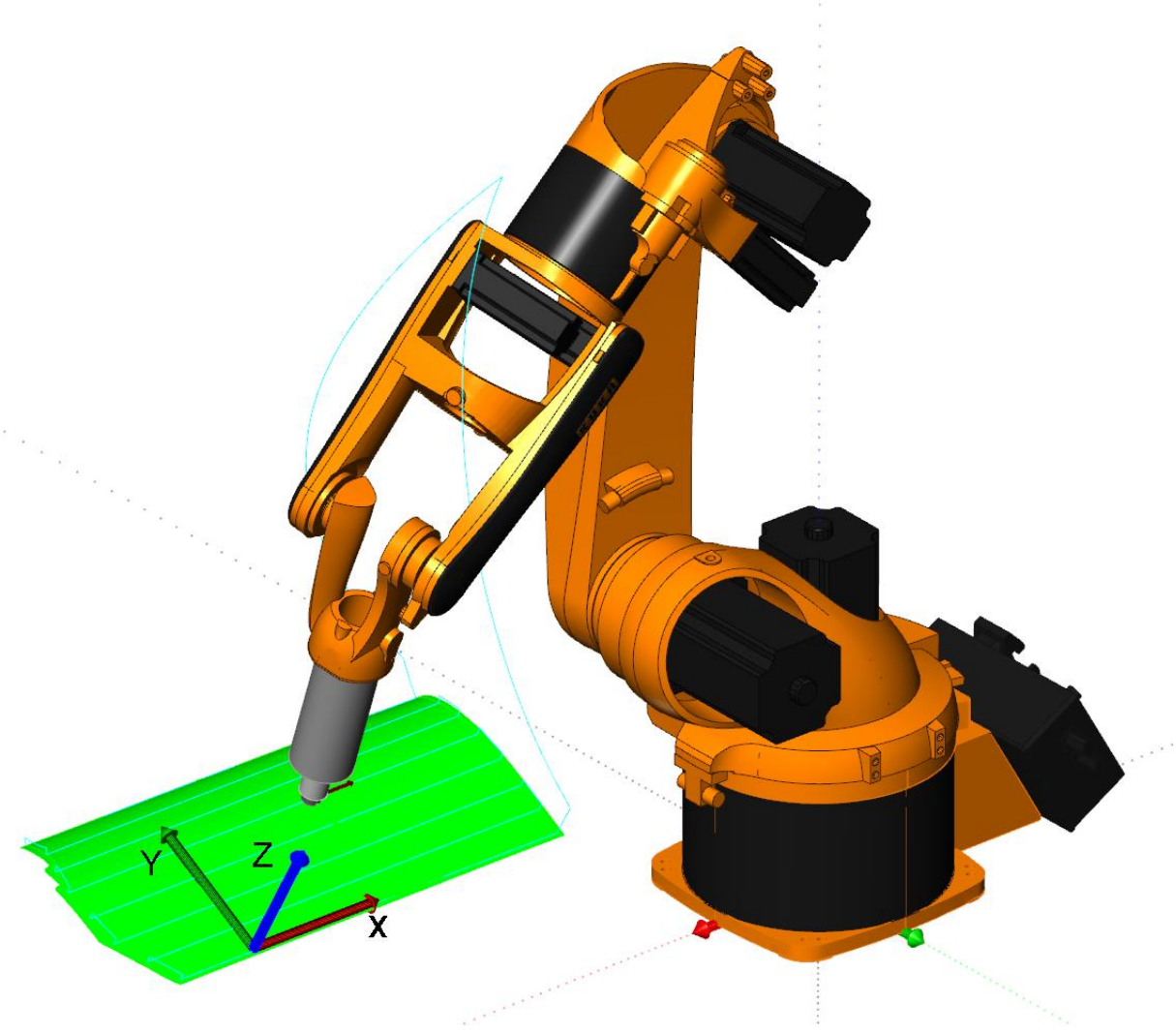

Figure 3. Simulated robotic NDT scan environment showing robotic arm in orange, test piece (leading edge skin) in green, scan path in turquoise, NDT probe and its holder in grey, base reference coordinate frame (arrows)

Scan path was further processed by Robotmaster (a C-hook in Mastercam), whereby actual scan and base frames are defined, as well as the scan rotation during the scan and the home position. Figure 3 illustrates simulated robotic NDT scan environment showing robotic arm (KUKA KR5 arc HW [18]) in orange, test piece (lead edge) in green, scan path in turquoise, NDT probe and its holder in grey as well as the base reference coordinate frame (arrows). For the sake of legibility of the illustration a large step size between longitudinal NDT probe passes was deliberately defined. It is possible to simulate any other robot in the library (Fanuc, ABB etc.) and there is a capability to add external axes (linear and rotary) and other CAD objects and accommodate interaction and collision avoidance etc. Next, the scan path is implemented in KUKA robot language (KRL) by means of the Robotmaster postprocessor and exported to the robot controller. The resulting .SRC file is fully editable, if required.

3. SFEC Setup and Robotic Scan Results

The procedure of the scan path generation described in section 2.2 was used for non-destructive scanning of a fixed leading edge skin panel by means of KUKA KR5 arc HW robot. The robotic arm was used to deploy an Eddy Current probe as shown in Figure 4. The respective robotic NDT scan of the leading edge skin was performed with a single element eddy current probe using Swept Frequency Eddy Current (SFEC) technique [19]. The probe had a ferrite pot core (external diameter 18 mm) and approximately 200 turns of winding. The probe was spring loaded. An Agilent 4395A Impedance Analyzer was used to produce excitation and read out serial impedance of the EC probe. Excitation frequencies were 100kHz, 200kHz, 300kHz and 400kHz. The effective scanning speed was approximately 5 mm/s. The robot controller transmitted actual probe position coordinates to an external PC via Ethernet RSI (robot-sensor interface) with interpolation cycle of 12 ms [20].

Results of the leading edge skin scan at 400 kHz excitation frequency are shown in Figure 5 (difference serial resistance R_s of the probe with respect to defect-free response) and Figure 6 (difference serial inductance L_s with respect to defect-free response). The EC signals are overlaid on CAD models (grey surface) performed in MatLab. Both rivets and rivet holes are clearly visible (compare with Fig.1). In addition,

the serial resistance map shows the presence of a subsurface stiffener (blue band along the second row of rivets from below). EC scan was carried at certain distance (about one half of the EC probe radius) from the edges in order to avoid strong signals due to edge effect.

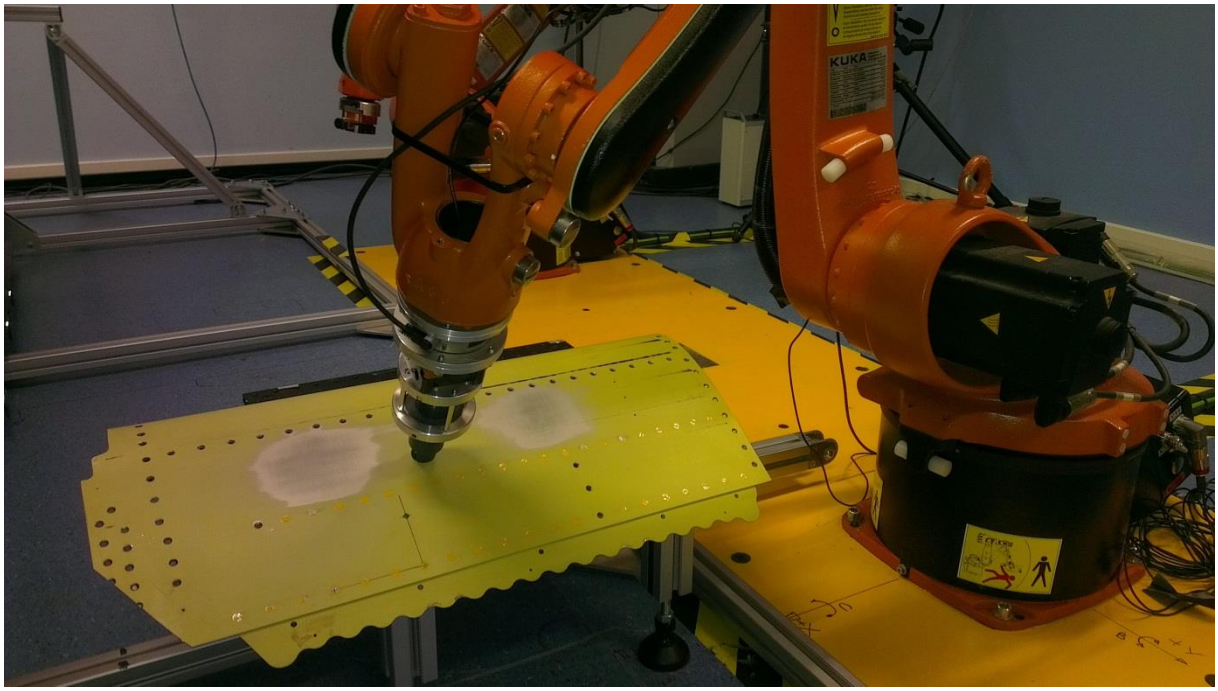

Figure 4. Illustration of practical implementation of the generated scan path for NDT of a fixed leading edge skin panel by means of KUKA KR5 arc HW robot

NDT response can also be imported in a CAD metrology software (e.g. Verisurf) as shown in Fig.7, colour map representing change of EC resistance at 400 kHz (compare with Fig.6).

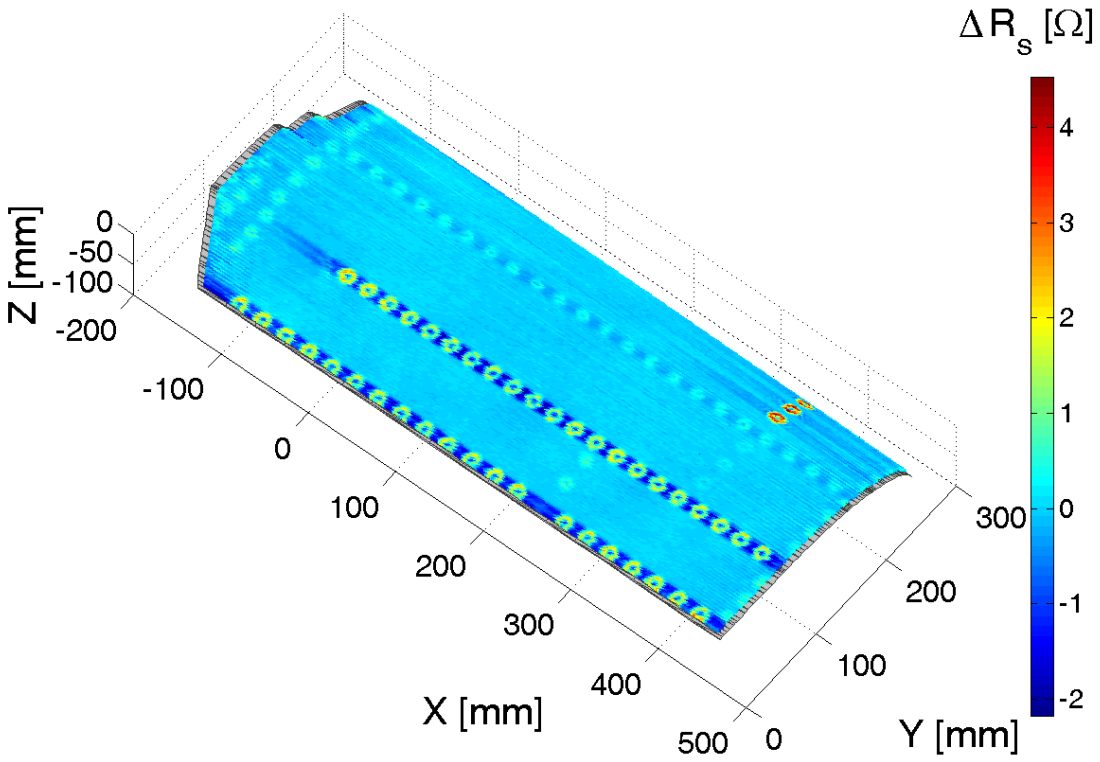

Figure 5. CAD overlay of EC resistance change during robotic scan of the edge skin at 400 kHz

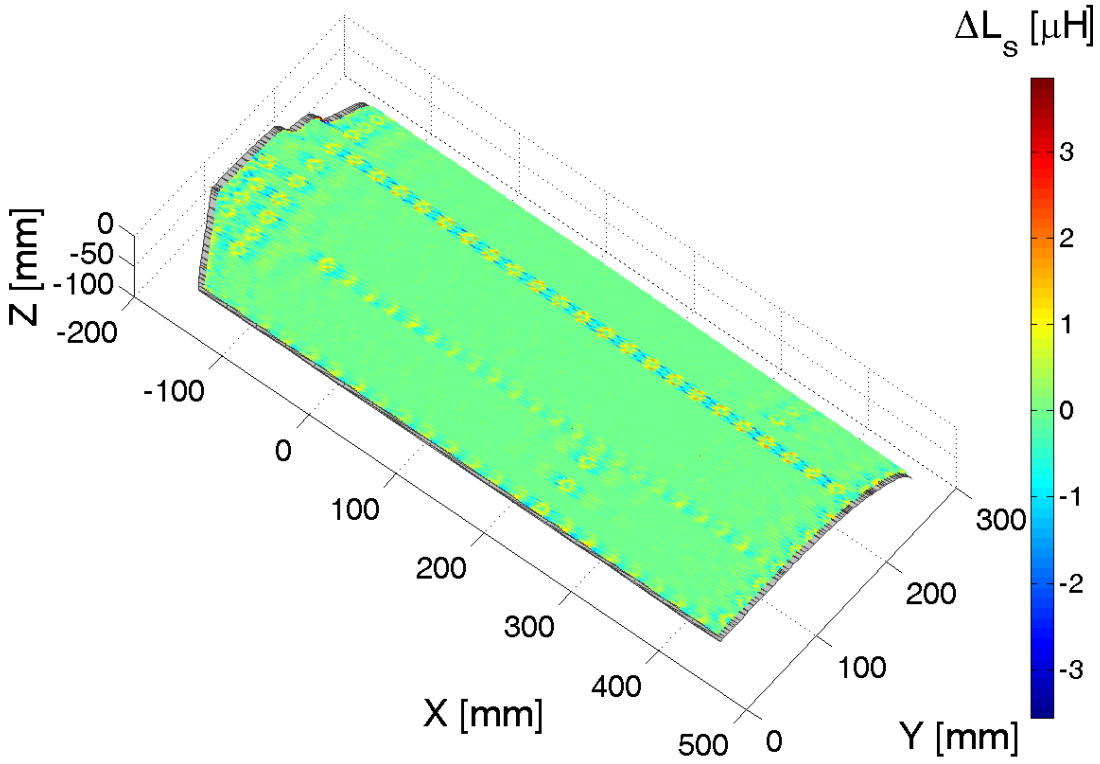

Figure 6. CAD overlay of EC inductance change during robotic scan of the edge skin at 400 kHz

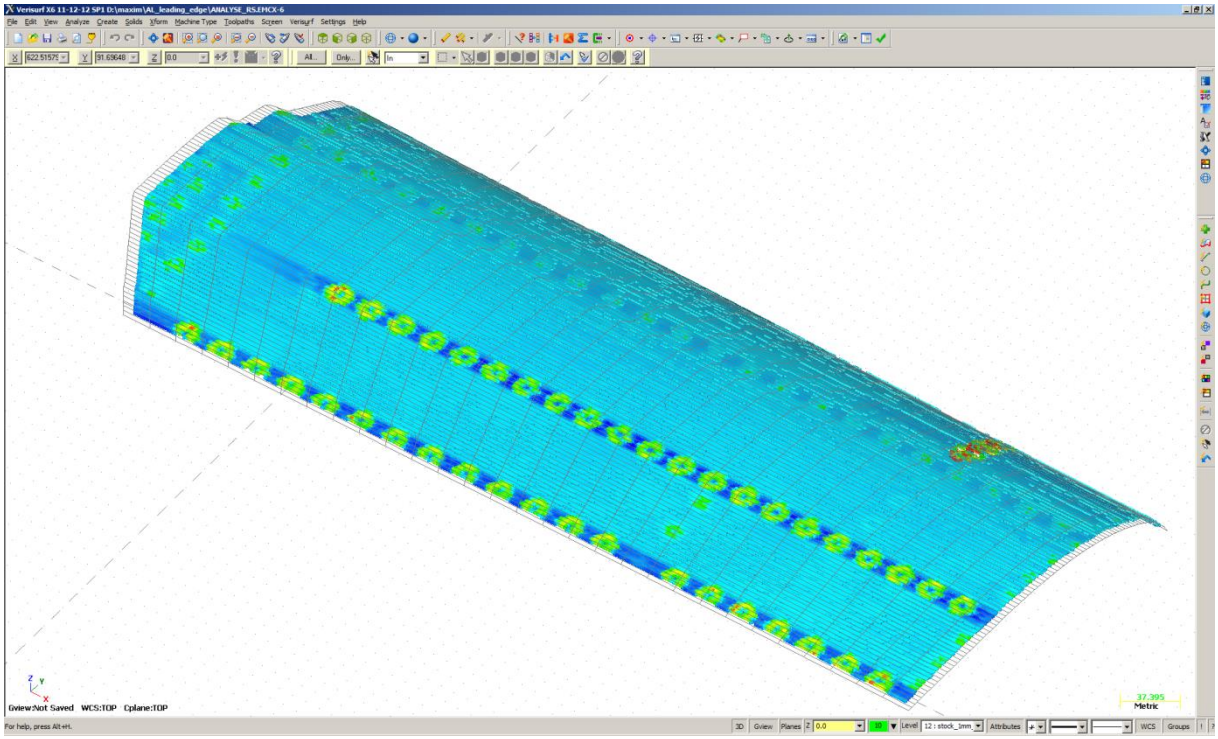

Figure 7. Overlay of NDT response at 400 kHz on CAD model in Verisurf metrology software

4. Path accuracy

As it was explicated in the Introduction, off-line robot programming imposes limitations on the path accuracy which is an important parameter of the robotic NDT inspection. ISO 9283:1998 "Manipulating industrial robots — Performance criteria and related test methods" [21] defines the path accuracy as the maximum path deviation along the path obtained in positioning and orientation. Positioning path accuracy is calculated as

$$AT_P = max\sqrt{(\bar{x}_i - x_{ci})^2 + (\bar{y}_i - y_{ci})^2 + (\bar{z}_i - z_{ci})^2}, i = 1...m, \quad (1)$$

where (x_{ci}, y_{ci}, z_{ci}) are the coordinates of the i-th point on the command path and ($\bar{x}_i$, $\bar{y}_i$, $\bar{z}_i$) are the corresponding coordinates of the i-th barycentre of the attained path. In our case, since the scan is unique, barycentre directly correspond to the attained path.

Orientation path accuracies AT_a, AT_b and AT_c are defined as the maximum deviations from commanded orientations about the x, y and z axes along the path, respectively:

$$AT_a = max|\bar{a}_i - a_{ci}|, i = 1 \ldots m, \quad (2)$$

where a_{ci} is the command orientation at the point (x_{ci}, y_{ci}, z_{ci}) and $\bar{a}_i$ is the average attained orientation angle at the *i*-th point of the path. In our case, since the scan is unique, the average orientations directly correspond to the attained path. Expressions similar to (2) are used for AT_b and AT_c.

First, path accuracy of the robot was measured according to ISO 9283:1998. Since the positional output of the robot encoders can be inaccurate due to deviations of the kinematic parameters [22], an external measurement system was used: an absolute laser tracker Leica AT901b [23]. The AT model available in our laboratory can only measure three degrees of freedom (DoF) and thus cannot be used to measure the orientation path accuracy. ISO 9283 prescribes four alternative paths which can be used to characterise a robot's path accuracy: a straight line, a rectangular path and two circular paths. The rectangular path was chosen since it is the morphologically closest to the scan path used to scan the leading edge skin panel. The followed path is shown in Figure 8. As prescribed by ISO 9283, the robot's Tool Centre Point (TCP) moved along the rectangular path at three override speeds: 10%, 50% and 100% of the rated velocity. Ten cycles were performed as required by the standard. The laser tracker acquired continuous readings of a Tool Ball Reflector (TBR) mounted at the TCP of the robot with time separation between readings being 1 ms, which is the highest acquisition rate of the AT901 sensor. Robot transmitted the command and the actual coordinates via Ethernet RSI interface to an external PC. The AT controller was programmed via emScon interface. Acquisitions from both the robot's controller and the AT controller were synchronised by means of a software trigger.

The path accuracy depends on the accuracy of the TCP calibration. TCP calibration is an operation the purpose of which is to determine the offset and orientation of the tool end point with respect to the robot's flange. A standard procedure of TCP calibration involves use of a solid spike as a reference point. A "laser spike" procedure was used for TCP calibration in this study: coordinates of the first (reference) position of the TCP (reflector) mounted onto the robot's flange were measured by the AT and stored in the

memory. Then, the reflector is brought to this point from other three sufficiently different directions. Current reflector coordinates are continuously programmatically compared with the memorised values until they coincide with a given tolerance. The tolerance was set 100 μm since a significantly lower tolerance would be unreasonably difficult to achieve since TCB calibration requires manual jogging of the robot. The reported TCP calibration uncertainty was 0.32 mm.

The laser tracker and the robot have intrinsic coordinate frames which in general do not coincide. In order to evaluate accuracy of a moving robot's TCP, coordinates of the laser tracker need to be transformed to the base coordinate system of the robot. For this purpose the robot's TCP was moved to three different points in the robot's working space, their respective coordinates were measured by both the laser tracker and the robot and the respective transformation matrix was determined. Coordinates transformation from the coordinate frame of the absolute laser tracker to the base coordinate frame of the robot was carried out by means of the homogeneous transformation [24]:

$$\begin{pmatrix} {}^{j}\boldsymbol{r} \\ 1 \end{pmatrix} = \begin{pmatrix} {}^{j}\boldsymbol{R}_i & {}^{j}\boldsymbol{p}_i \\ \mathbf{0}^{\mathrm{T}} & 1 \end{pmatrix} \begin{pmatrix} {}^{i}\boldsymbol{r} \\ 1 \end{pmatrix}, \tag{3}$$

where ${}^{i}\boldsymbol{r}$ and ${}^{j}\boldsymbol{r}$ are the position vectors in the AT and robot coordinate frames, respectively, ${}^{j}\boldsymbol{R}_i$ is the rotation matrix of the frame *i* relative to coordinate frame *j* and ${}^{j}\boldsymbol{p}_i$ is the position vector of the origin of the frame *i* relative to coordinate frame *j*.

Figure 8 shows shape of the test path as measured at 100% rated speed showing command coordinates and actual coordinates reported by the robot's encoders as well as the transformed coordinates measured with the laser tracker. Table 1 presents the calculated path accuracy for the three rated speeds. As expected, error increases with the higher speed.

Table 1. Path accuracy AT_p (mm) according to ISO 9283:1998

@10% of rated velocity	**@50% of rated velocity**	**@100% of rated velocity**
1.844	3.178	4.464

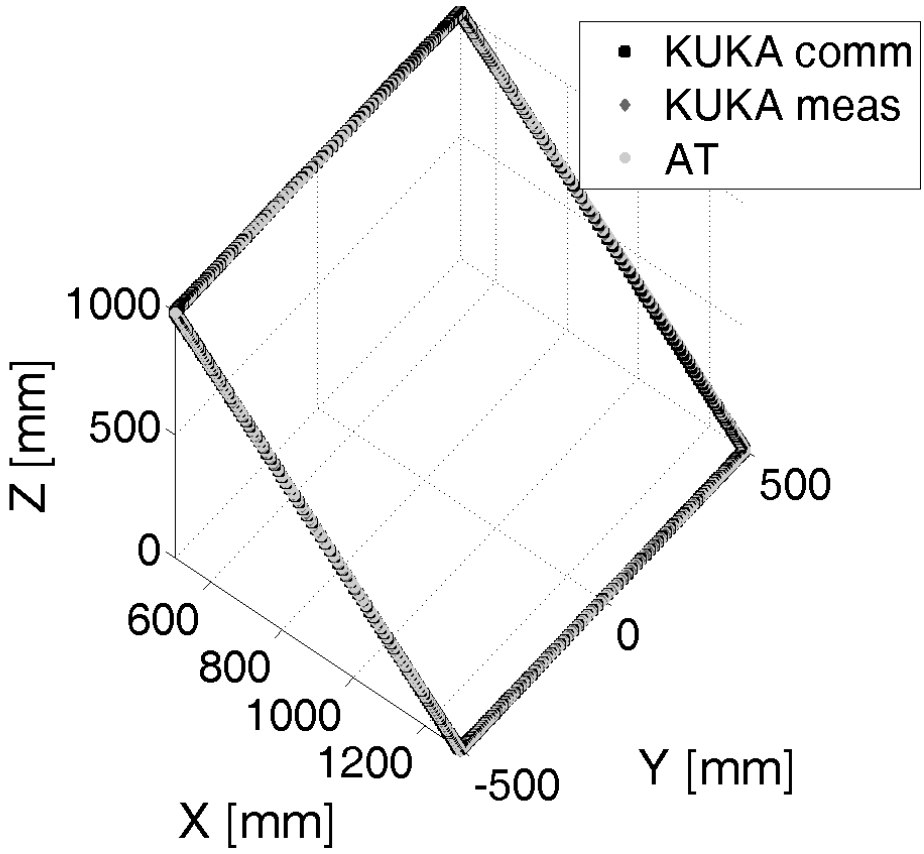

Figure 8. Shape of the test path as measured at 100% rated speed showing command coordinates and actual coordinates reported by the robot's encoders as well as the transformed coordinates measured with the laser tracker

Having determined path accuracy of the robot along a path prescribed by ISO 9283:1998, path accuracy of the robot along the generated scan path for NDT of the aluminium leading edge skin panel the was measured as well. The TBR was mounted at the TCP and the NDT scan path was executed at 10%, 50% and 100% of the rated velocity. The coordinates measured using the laser tracker were compared with the command path coordinates acquired from the robot's controller via RSI. Figure 9 shows the resulting distribution map of the positional error at 100% of the rated velocity when the deviations are biggest (see Table 2). Component-wise, the major positional error is exhibited in the scan direction. That is, coordinate X has the biggest error along the passes and coordinate Y has the biggest error when the probe moves between the passes, which results in bigger errors at the scan area edges along X axis. Table 2 presents calculated path accuracy using formula (1). The positional accuracy of

continuous motion inversely depends on the motion speed; that is the faster is the motion, the bigger position error ensues. In order to compensate for the pose error, output of the laser tracker or other metrological system can be used to produce feed-back to the motion planner of the robot via RSI. Inaccuracies presented in Table 2 are somewhat lower than the corresponding values in Table 1 which can be due to the fact that the NDT scan pass has a significantly smaller extent than the path prescribed by ISO 9283:1998 The scanned part was also located closer to the central area of the working envelope of the robot whereas bigger inaccuracies can be expected at the extremes of the robot's reach. Thus the NDT scan path does not represent accuracy over the entire working envelope of the robot.

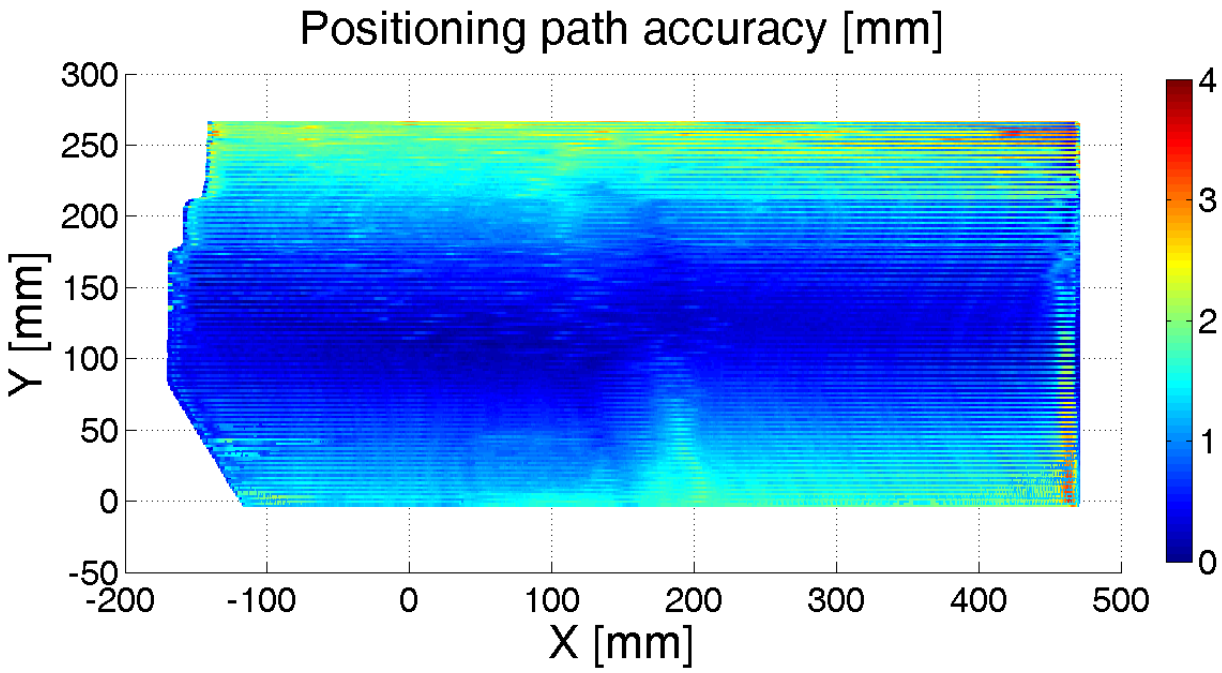

Figure 9. Positional error measured along the generated NDT scan path at 100% rated speed

Table 2. Path accuracy (mm) measured along the NDT scan path

@10% of rated velocity	**@50% of rated velocity**	**@100% of rated velocity**
1.493	3.464	3.528

Path accuracy calculated in accordance with ISO 9283:1998 is by definition the maximum error of the respective pose component and thus

the average positional error shown in Figure 9 is less severe than AT_p. Moreover, only scan at 10% of the rated velocity can produce NDT responses with sufficient spatial resolution (2 mm in the presented study), measurements at 50% and 100% of the rated velocity were carried out for comparison. The standard deviation of the attained path from the command path at 10% of the rated velocity was calculated to be below 0.35 mm. Taking in account errors resulting from the reverse engineering of the surface of the leading edge skin panel and error due to TCP calibration the positional uncertainty of the NDT scan does not exceed 0.5 mm. The path deviations did not result in major noise in the EC response due to the lift-off variation. Comparable results are found in [25], where a different NDT technique (ultrasonic phased array) was used; the authors of this work obtained a standard deviation of 2.33 mm and an average standoff error of 0.83 mm, when using commercial path-planning software in conjunction with the original CAD model of a large composite material sample with complex geometry.

5. Conclusions

This paper presented development of a new robotic NDT scanning capability of curved surface test-pieces using industry standard tools which include industrial robots and off-line programming CAD/CAM software. Due to the absence of a CAD model of the part reverse engineering of the part was performed using standard surface metrology instrumentation. To illustrate the successful delivery of the NDT measurement, a single element eddy current probe was used with a KUKA KR5 robot to scan an aluminium leading edge skin panel. However, the presented approach can be applied to arrays of sensors of any type. The only parameter which will change is the step between scan passes. Positioning accuracy of the robot and of the performed continuous scan was measured in accordance with ISO 9283:1998 using an external laser tracker. The maximum positioning path inaccuracy AT_p according to ISO 9283:1998 was found to be circa 1.5 mm when scanning at 10% of the robot's rated velocity. The positional uncertainty of the NDT scan calculated as the standard deviation of the measured path coordinates from the command path coordinates does not exceed 0.5 mm which is

rather moderate taking in account uncertainties associated with the off-line robot programming. The path deviations did not result in major noise in the EC response due to the lift-off variation. Our future work will be aimed at implementation of on-line correction of the robot trajectory based on live feedback obtained through the NDT probes and/or through additional sensing strategies (e.g. laser profilers, force-torque sensors, etc.).

Acknowledgements

This work was supported by EPSRC, EP/F017332/1, "UK Research Centre in NDE.

References

[1] UK Research Centre in Nondestructive Evaluation.
[2] Bridge B, Sattar T, Chen S, Khalid A. On the design of multi-task, compact, climbing robotic NDT systems for remote operation on large surfaces and in hazardous environments. Nondestructive Testing and Evaluation. 1997;13:85-111.
[3] Smith RA, Harrison DJ. Hall sensor arrays for rapid large-area transient eddy current inspection. Insight. 2004;46:142-6.
[4] Lines DIA. Rapid distributed data collection with arrays - the next step beyond full waveform capture. Insight. 2006;48:84-8.
[5] Moon W. Improving NDI productivity via standardized robotic platforms. International SAMPE Technical Conference2013. p. 2116-25.
[6] Moon WJ. Improving NDI productivity via standardized robotic platforms. International SAMPE Symposium and Exhibition (Proceedings)2010.
[7] Wright B, Cooper I, Nicholson PI, Mineo C, Pierce SG. PAUT Inspection of Complex Shaped Composite Materials through 6 DOFs Robotic Manipulators. 53rd Annual Conference of The British Institute of Non-Destructive Testing (NDT 2014). Manchester, UK2014.
[8] Morozov M, Rubinacci G, Tamburrino A, Ventre S. Electromagnetic Non-Destructive Evaluation Of Reinforced Concrete Rebars. In: A. Tamburrino YM, Z.

Chen and L. Udpa, editor. Electromagnetic Nondestructive Evaluation: IOS Press, Amsterdam; 2008. p. 263 – 70.
[9] Morozov M, Rubinacci G, Tamburrino A, Ventre S. Evaluation Of Subsurface Cracks In Riveted Aluminium Joints Using Industrial Eddy Current Instrumentation. In: A. Tamburrino YM, Z. Chen and L. Udpa, editor. Electromagnetic Nondestructive Evaluation: IOS Press, Amsterdam; 2008. p. 187 – 94.
[10] Sattar TP, Brenner A-A. Robotic system for inspection of test objects with unknown geometry using NDT methods. The Industrial Robot. 2009;36:340-3.
[11] Rohmann. EloScan Technical Data. Rohmann GmbH.
[12] Stetson JT, De Odorico W. Robotic inspection of fiber reinforced composites using phased array UT. AIP Conference Proceedings2014. p. 1889-95.
[13] Composite Inspection | GE Measurement & Control.
[14] Olivieri P, Birglen L, Maldague X, Mantegh I. Coverage path planning for eddy current inspection on complex aeronautical parts. Robotics and Computer-Integrated Manufacturing. 2014;30:305-14.
[15] Wittenberg G. Developments in offline programming: An overview. Industrial Robot. 1995;22:21-3.
[16] Carter S. OFF-LINE ROBOT PROGRAMMING: THE STATE-OF-THE-ART. Industrial Robot. 1987;14:213-5.
[17] Roos E, Behrens A. Off-line programming of industrial robots — Adaptation of simulated user programs to the real environment. Computers in Industry. 1997;33:139-50.
[18] KUKA. KR5 arc HW datasheet. KUKA systems.
[19] Morozov M, Tian GY, Edgar D. Comparison Of Pec And Sfec Nde Techniques. Nondestructive Testing and Evaluation. 2009;24:153-64.
[20] KUKA. KUKA.RobotSensorInterface 2.3. KUKA systems.
[21] ISO 9283:1998(en) Manipulating industrial robots — Performance criteria and related test methods.
[22] Slamani M, Nubiola A, Bonev I. Assessment of the positioning performance of an industrial robot. Industrial Robot. 2012;39:57-68.
[23] Leica-Geosystems. Leica Absolute Tracker AT901.
[24] Springer Handbook of Robotics: Springer-Verlag Berlin Heidelberg; 2008.

[25] Mineo C, Pierce S G, Nicholson P I, and Cooper I. Introducing a novel mesh following technique for approximation-free robotic tool path trajectories. Journal of Computational Design and Engineering 4, no. 3 (2017): 192-202.